Journal of Magnetism and Magnetic Materials 346 (2013) 118–123

Contents lists available at SciVerse ScienceDirect

Journal of Magnetism and Magnetic Materials

journal homepage: www.elsevier.com/locate/jmmm

Magnetic separation of particles and cells in ferrofluid flow through a straight microchannel using two offset magnets

Jian Zeng [a], Yanxiang Deng [a], Pallavi Vedantam [b], Tzuen-Rong Tzeng [b], Xiangchun Xuan [a,*]

[a] Department of Mechanical Engineering, Clemson University, Clemson, SC 29634-0921, USA
[b] Department of Biological Sciences, Clemson University, Clemson, SC 29634-0314, USA

ARTICLE INFO

Article history:
Received 23 April 2013
Received in revised form
6 July 2013
Available online 16 July 2013

Keywords:
Microfluidics
Ferrofluid
Particle separation
Magnetophoresis
Lab on a chip

ABSTRACT

The separation of particles and cells is critical in many chemical and biological applications. This work presents a simple idea for utilizing a pair of permanent magnets to continuously separate diamagnetic particles and cells in ferrofluid flow through a straight microchannel. The first magnet is placed close to the microchannel for focusing the particle mixture to a single stream without the use of a sheath flow. The second magnet, which is offset from the first magnet and placed farther from the channel, is to displace the aligned particles to dissimilar flow paths for a continuous sorting. This idea is first demonstrated through the separation of 3 μm- and 10 μm-diameter polystyrene particles, where the effects of flow speed and magnet distance are both examined. The experimental data are found to fit well with the predictions of an analytical model. Furthermore, a continuous separation of live yeast cells from 10 μm polystyrene particles is implemented in the same device.

1. Introduction

Separating particles and cells is often necessary in a variety of chemical and biological applications. Starting from a sample mixture, particles of distinguishable properties (e.g., size, density, charge and shape) may be continuously separated and sorted by means of an externally provided or internally induced force field. Among these are electric [1,2], magnetic [3,4], acoustic [5,6], optical [7,8], and hydrodynamic [9,10] methods, all of which have been and will continue being the research foci in microfluidic devices for diverse lab-on-a-chip applications [11–15]. However, many of these continuous methods catered towards particle separation have a burdened secondary effect of requiring expensive equipment and/or complicated device fabrication etc. In contrast, with utilizing permanent magnets that naturally produce their own magnetic field, magnetic separation techniques exhibit a number of advantageous features such as low cost (cheap magnets off-the-shelf) and unwanted fluid heating issues [16–20].

Magnetic field-induced particle and cell separation has been implemented in primarily two modes [21,22]. The first mode works primarily for the separation of magnetic particles (or magnetically tagged bioparticles) from diamagnetic (or non-magnetic as often called) particles, where the former are first retained by a magnet and later released by removing the magnetic field after diamagnetic particles have all flown through the retention chamber [23,24]. One such example is magnetic-activated cell sorting (MACS) [25], which obviously takes place in a batch process. Other notable batchwise magnetic separations were reported by Yellen et al. [26] and Kose et al. [27] through the use of travelling-wave magnetic field. In the former study, superparamagnetic particles can be size-selectively locked onto patterned micro-magnets by varying the driving frequency of an external rotating magnetic field [26]. A similar idea was later employed by Kose et al. [27] to selectively trap and sort diamagnetic particles and cells in ferrofluid based on size, shape and elasticity using on-chip current carrying electrodes-generated travelling-wave magnetic field gradients.

In the second mode of magnetic separations, the particle mixture suspension is confined by a co-flowing buffer solution, upon which a transverse magnetic force deflects particles to distinct flow paths in the buffer solution. Such a continuous-flow method has been demonstrated to separate magnetic (or tagged) particles from diamagnetic particles by using either an external magnet (permanent or electric current-induced) itself [28–30] or external-magnet excited microfabricated soft magnets [31–33]. It can also work for the continuous separation of magnetic particles by size and/or magnetization, which, termed free-flow magnetophoresis [34], has been demonstrated by Pamme and her colleagues [35,36] and later applied to separate magnetically-labeled cells [37,38]. Moreover, the same approach has recently been applied to separate diamagnetic particles in magnetic solutions including paramagnetic solutions by Pamme's group [39,40] and ferrofluids by Mao's group [41,42]. The main drawback of this continuous magnetic separation technique lies in the use of a sheath

* Corresponding author. Tel.: +1 864 656 5630; fax: +1 864 656 7299.
E-mail address: xcxuan@clemson.edu (X. Xuan).

0304-8853/$ - see front matter © 2013 Elsevier B.V. All rights reserved.
http://dx.doi.org/10.1016/j.jmmm.2013.07.021

fluid, which complicates the flow control and meanwhile dilutes the sorted particles.

To date, there has been little work reported on continuous-flow sheath-free magnetic separation of particles. Our group has recently demonstrated the use of a U-shaped microchannel to sort particles with a single permanent magnet [43]. This approach exploits the induced negative or positive magnetophoretic deflection to focus diamagnetic or magnetic particles to a single stream in the first branch of the U-channel without a sheath flow and then separate them continuously in the second branch. In this work, we present another simple method for diamagnetic particle and cell separation in ferrofluid flow through a straight microchannel. The use of two offset magnets enables particle focusing and separation in a single fluid flow while providing the flexibility to vary the magnet position for accommodating particles of various sizes. This technique is demonstrated through the sorting of polystyrene particles and yeast cells. An analytical model is also developed to simulate the magnetic control of particle transport and separation in ferrofluid microflows.

2. Experiment

The standard soft lithography method was used to fabricate the straight microchannel with polydimethylsiloxane (PDMS). Detailed procedures for channel fabrication can be referred to Zeng et al. [44]. The rectangular cross-sectioned microchannel has a length of 2.5 cm, width of 200 μm, and depth of 25 μm. There are four rectangular blocks designed at each of the two reservoir-microchannel junctions, which serve to filter out particle aggregates and PDMS debris at the inlet and provide distinct flow passages for sorted particles and cells at the outlet. Two equal and opposing Neodymium–Iron–Boron (NdFeB) permanent magnets (B221, 1/8 in. × 1/8 in. × 1/16 in., K&J Magnetics Inc.) were imbedded in the PDMS slab with their magnetization directions perpendicular towards the microchannel. As shown in Fig. 1, the device has its first magnet placed 500 μm (edge to edge) away from the microchannel. The second magnet, which is 1 mm offset from the first one along the flow direction, stays further away from the microchannel with a distance being variable in experiments.

A commercially available water-based ferrofluid, EMG 408 (Ferrotec Corp.), was diluted with deionized water (Fisher Scientific) to 0.05 × its original concentration (1.2% magnetic nanoparticles in volume). To show evidence of size-based separation, 3 μm and 10 μm-diameter diamagnetic polystyrene particles (Thermo Fisher Scientific) were re-suspended in the diluted ferrofluid at a concentration of 5×10^6 and 4×10^5 particles/ml, respectively. Live yeast cells (*Saccharomyces cerevisiae*) were cultured overnight in Sabouraud's dextrose broth in a shaker incubator at 30 °C, and were re-suspended in sterile phosphate buffered saline (PBS) solution to a concentration of 6.85×10^8 cells/ml. Prior to use, yeast cells were washed with deionized water three times and re-suspended in 0.05 × EMG 408 ferrofluid along with 10 μm particles at similar concentrations mentioned above. The measured diameter of yeast cells is 5 μm in approximation. Tween 20 (Fisher Scientific) was added to both the particle and cell suspensions at 0.1% by volume to minimize their aggregations and adhesions to microchannel walls.

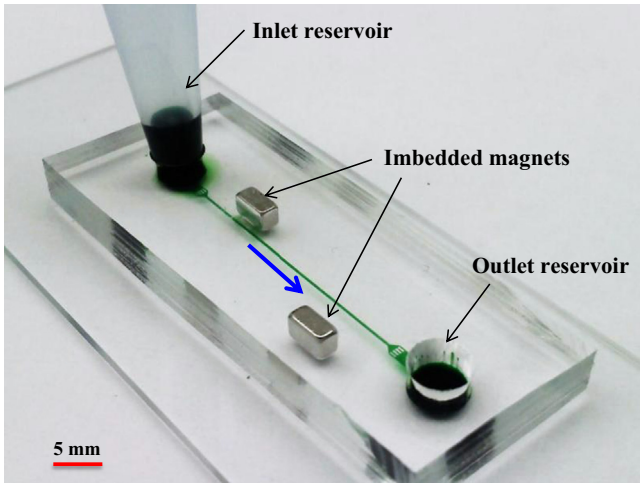

Fig. 1. Picture of the experimental microfluidic device with the straight microchannel and reservoirs filled with green food dye for clarity. The block arrow indicates the flow direction in the demonstrated diamagnetic particle and cell separation experiments. (For interpretation of the references to color in this figure legend, the reader is referred to the web version of this article.)

The microchannel was rinsed thoroughly after its fabrication and prior to experiment. A standard 1-ml pipette tip was used to elevate the fluid height in the inlet reservoir in order to produce a pressure driven flow (see Fig. 1). Adjusting this fluid height provides an easy control of the flow speed. To reduce the effects of back-flow on particle/cell separation, the outlet reservoir was made large and manually kept free of fluid buildup during experiment using a pipette. As the diluted ferrofluid appears transparent in microchannels, the suspended particles and cells can be viewed without the need of fluorescent labeling. The particle and cell motion was visualized using an inverted microscope (Nikon Eclipse TE2000U, Nikon Instruments, Lewisville, TX) under a bright-field illumination. Digital videos (at a time rate of around 12 frames per second) and images were recorded through a CCD camera (Nikon DS-Qi1Mc) and post-processed using the Nikon imaging software (NIS-Elements AR 2.30).

3. Theory

3.1. Diamagnetic particle/cell separation mechanism

Diamagnetic particles and cells undergo negative magnetophoresis in a ferrofluid when subjected to a non-uniform magnetic field. This motion, $\mathbf{U}_m$, is directed towards the decreasing magnetic field and is expressed by [45,46]

$$\mathbf{U}_m = \frac{-\mu_0\phi a^2}{9\eta f_D}\frac{M_d L(\alpha)\nabla\mathbf{H}^2}{H} \tag{1}$$

$$L(\alpha) = \coth(\alpha) - \frac{1}{\alpha} \quad \text{and} \quad \alpha = \frac{\pi\mu_0 M_d H d^3}{6k_B T} \tag{2}$$

where μ_0 is the permeability of free space, ϕ is the volume fraction of magnetic nanoparticles in the ferrofluid with M_d being their saturation moment, a is the radius of diamagnetic particles or cells, η is the ferrofluid viscosity, f_D is the drag coefficient accounting for the wall retardation effects [47–49], $L(\alpha)$ represents Langevin function [50], $\mathbf{H}$ is the magnetic field with a magnitude of H, d is the average diameter of magnetic nanoparticles, k_B is the Boltzmann constant, and T is the ferrofluid temperature. Note that while the ferrofluid is diluted in the current work, its magnetization is still much larger than that of the diamagnetic particles and cells under uses. Therefore, the contribution of the latter to the magnetophoretic particle velocity, $\mathbf{U}_m$ in Eq. (1), has been neglected [45–49]. The dependence of $\mathbf{U}_m$ on the particle radius squared enables the separation of diamagnetic particles and cells by size.

Fig. 2 shows schematically the separation mechanism of diamagnetic particles and cells in ferrofluid flow through a straight microchannel. As seen from the magnetic field contour (represented by the background color, the darker the larger), the two offset magnets (see a picture of the device in Fig. 1) each creates its own magnetic field gradients within the ferrofluid. However, as the first magnet is placed closer to the microchannel, the induced magnetophoretic velocity, $\mathbf{U}_m$, (see the arrows in Fig. 2), is larger than that in the second magnet region. Thus, at an appropriate

ferrofluid flow, $\mathbf{U}_f$, different sizes of particles in a uniform mixture can all experience a full deflection across the channel width after passing through the stronger first-magnet field. Entering the weaker second-magnet field, however, $\mathbf{U}_m$ becomes noticeably discriminatory towards the size of the particles, thereby displacing larger particles farther than compared to smaller ones. The consequence is a separation of the focused particle mixture into two or more (if more than two sizes of particles are present in the suspension) sub-streams exiting the microchannel. The best scenario for this continuous size-based diamagnetic particle separation is that the larger particles (for a binary separation) can still achieve a full-width deflection in the second-magnet field, which will be presented in the results section (*c.f.* Fig. 4).

3.2. Simulation of diamagnetic particle/cell trajectories

A 3D analytical model was developed to simulate the magnetic transport and separation of diamagnetic particles and cells in ferrofluid flow through the uniform part of the straight microchannel in Fig. 1. The instantaneous position of a particle, $\mathbf{r}_p$, was obtained by integrating the particle velocity over time,

$$\mathbf{r}_p = \mathbf{r}_0 + \int_0^t [\mathbf{U}_f(t') + \mathbf{U}_m(t')]dt' \quad (3)$$

where $\mathbf{r}_0$ is the initial position of the particle center, t is the time coordinate, and $\mathbf{U}_f$ is the ferrofluid velocity. The buoyancy and inertial effects on particle velocity are both excluded in Eq. (3) because the particle density is approximately the same as the ferrofluid density [45] and the Reynolds number is very small under the experimental conditions. The ferrofluid flow in the microchannel is assumed fully developed and not affected by the particle motion. Hence, the flow velocity can be expressed by the analytical formula for pressure-driven flow in a rectangular channel [45,47–49]. The pressure gradient involved in the formula was determined by measuring the fluid height in the inlet reservoir (see Fig. 1). The magnetophoretic particle velocity, $\mathbf{U}_m$, was calculated from Eq. (1), where the magnetic field of the two offset magnets was computed from Furlani's analytical formula [51]. A custom-written Matlab® program was employed to simulate and plot the particle trajectory, which was described in detail in our earlier work [45,49] and skipped here for brevity.

4. Results and discussion

4.1. Magnetic separation of polystyrene particles

Fig. 3 demonstrates the magnetic separation of 3 μm and 10 μm polystyrene particles in 0.05× EMG 408 ferrofluid with an average flow speed of 0.6 mm/s. The first and second magnets were respectively placed 500 μm and 2600 μm away, edge to edge, from the microchannel. The streak image in Fig. 3(a), which was obtained by superimposing a sequence of snapshot images, shows a mixture of the two sizes of particles entering into the microchannel with uniformly scattered positioning over the channel width. In contrast, the streak image in Fig. 3(c) shows the same binary mixture of particles exiting the main length of the microchannel along distinct flow paths. The development of this continuous particle separation process is illustrated in Fig. 3(b) (top row for experimentally obtained streak images and bottom row for theoretically predicted particle trajectories).

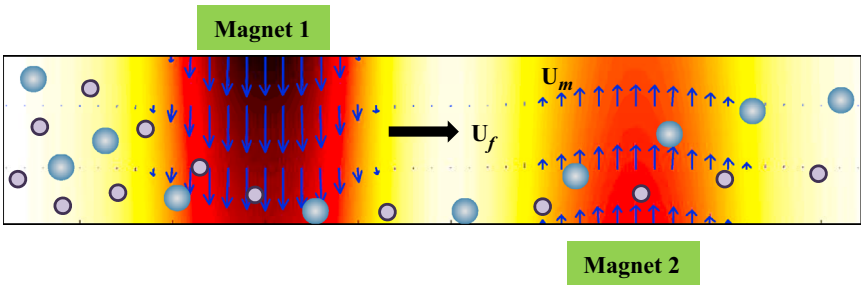

Fig. 2. Schematic illustration of the mechanism for diamagnetic particle and cell separation in ferrofluid flow through a straight microchannel using two offset magnets (not drawn to scale). The background color shows the magnetic field contour (the darker color, the larger magnitude). The thin arrows indicate the direction and magnitude (by the length) of the induced magnetophoretic particle velocity, $\mathbf{U}_m$. The block arrow indicates the direction of the ferrofluid flow, $\mathbf{U}_m$. The mixture of particles experiences a full deflection after passing through the stronger first-magnet field, and is then split into two sub-streams in the weaker second-magnet field due to the particle size dependence of $\mathbf{U}_m$. (For interpretation of the references to color in this figure legend, the reader is referred to the web version of this article.)

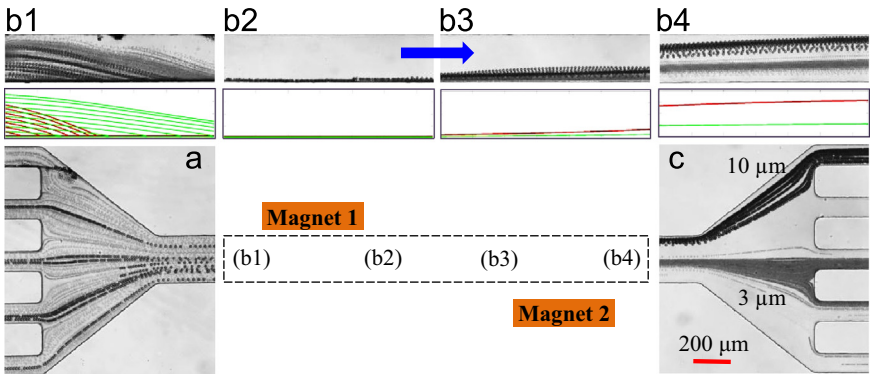

Fig. 3. Illustration of the continuous magnetic separation of 3 μm and 10 μm polystyrene particles in 0.05× EMG 408 ferrofluid at an average flow speed of 0.6 mm/s. Magnets 1 and 2 are placed 500 μm and 2600 μm away from the microchannel, respectively. (a) and (c) show the particle streak images at the inlet and outlet of the microchannel respectively. (b) compares the experimental (top row) and theoretical (bottom row, red lines for 10 μm particles and green lines for 3 μm ones) results of particle trajectories in a series of four viewing windows with their relative positions to the two magnets indicated in the figure (not drawn to scale). The block arrow indicates the flow direction. (For interpretation of the references to color in this figure legend, the reader is referred to the web version of this article.)

The relative positions of the four viewing windows (b1–b4) with respect to the two magnets are schematically shown in the bottom-middle panel of Fig. 3.

At the leading edge of the first magnet, see Fig. 3(b1), 3 μm and 10 μm particles are both deflected away from the magnet by negative magnetophoresis. However, the deflection of 10 μm particles takes place at a higher rate due to their larger magnetophoretic velocity than 3 μm particles. After the rear edge of magnet 1 in Fig. 3(b2), both sizes of particles obtain a full-width deflection and migrate in a tight stream adjacent to the channel sidewall. Fig. 3(b3) shows that the two particles begin to be separated at the leading edge of the second magnet due to their dissimilar deflection rates. The separation gap increases as particles travel past this magnet, which is demonstrated by the streak image after the rear edge of magnet 2 in Fig. 3(b4). The theoretically predicted trajectories of 3 μm (green lines) and 10 μm (red lines) particles under the experimental conditions are presented in the bottom row of Fig. 3(b), which show reasonable agreement with the experimentally obtained particle streak images in the top row. A quantitative comparison between experiment and modeling is given below for examining the effects of flow speed and magnet-channel distance on particle separation.

Fig. 4(a1, a2 and a3) compares the separation images of 3 μm and 10 μm particles at the channel outlet under the average ferrofluid speeds of 0.6, 0.8, and 1.2 mm/s, respectively. The relative positions of the sorted particles with respect to the channel centerline, i.e., the dash-dotted line in Fig. 4(a), are measured from the streak images directly and presented as symbols (hollow for 3 μm and filled for 10 μm) in Fig. 4(b). The vertical error bar for each symbol spans the width range of the corresponding particle stream in the image. The horizontal error bars are estimated from the experimental error in measuring the fluid height in the inlet reservoir. The dashed and solid lines in Fig. 4(b) represent the theoretically predicted positions of 3 μm and 10 μm particles, respectively. A good quantitative agreement is seen in between the experimental and theoretical results. As the trend shows, the separation gap between the two particle-streams increases with a decrease in the flow speed. It reaches the maximum when 10 μm particles get nearly a full deflection in the second magnet, which, based on the modeling, occurs at about an average flow speed of 0.5 mm/s. Further lowering the flow speed will, however, decrease the separation gap because 3 μm particles can still gain a magnetic deflection but not 10 μm ones.

We also examined the effects of the second magnet-microchannel distance on the separation gap between 3 μm and 10 μm particles while fixing the first magnet distance at 500 μm. The average flow speed of the suspending 0.05 × EMG 408 was maintained at 1.2 mm/s for a fair comparison. The results of this study are shown in Fig. 5, where the solid line presents the theoretical prediction and symbols represent the measured center-to-center distances of the sorted particle streams in the inset streak images. The vertical error bars for the experimental data cover the range from the minimum to the maximum edge-to-edge distance of the two particle streams. As expected, with a smaller distance for the second magnet, the separation gap between the two sizes of particles is increased and so the separation efficiency is improved. Moreover, the experimental results are predicted by the analytical model with a reasonable accuracy. In addition, it is important to note that the particle separation gap can also be affected by the distance between the second magnet and the channel outlet. This holds true as long as the distance is within the working range of the second magnet, which is estimated to be around 1 mm from the magnet surface. We should make use of this entire distance for enhanced particle separation.

4.2. Magnetic separation of live yeast cells from polystyrene particles

Fig. 6 shows the streak images for magnetic separation of live yeast cells and 10 μm polystyrene particles at the inlet (left) and

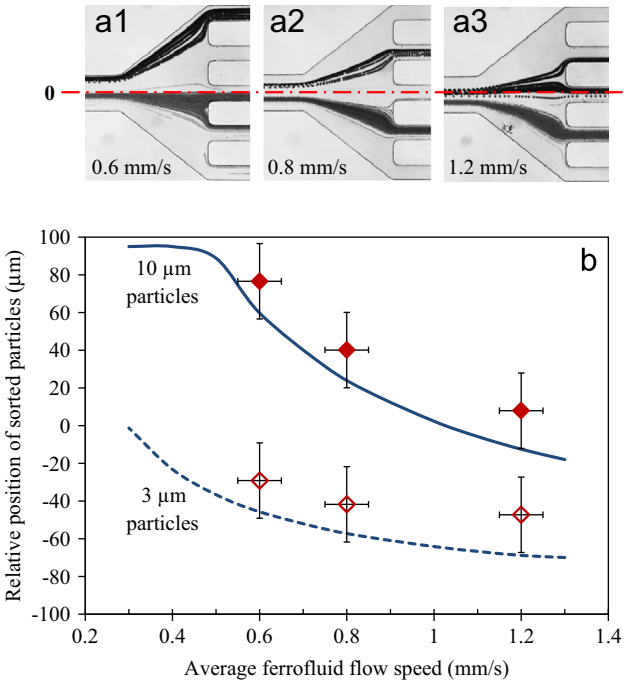

Fig. 4. Ferrofluid speed effects on the magnetic separation of 3 μm and 10 μm polystyrene particles: (a1)–(a3) show the streak images at the outlet of the straight microchannel under the average flow speed of 0.6 mm/s (a1), 0.8 mm/s (a2), and 1.2 mm/s (a3) (other conditions are referred to Fig. 3); (b1)–(b4) compare the experimental (symbols) and theoretical (lines) data for the relative positions of the sorted particles with respect to the channel centerline [highlighted by the dash-dotted line in (a)] at various flow speeds.

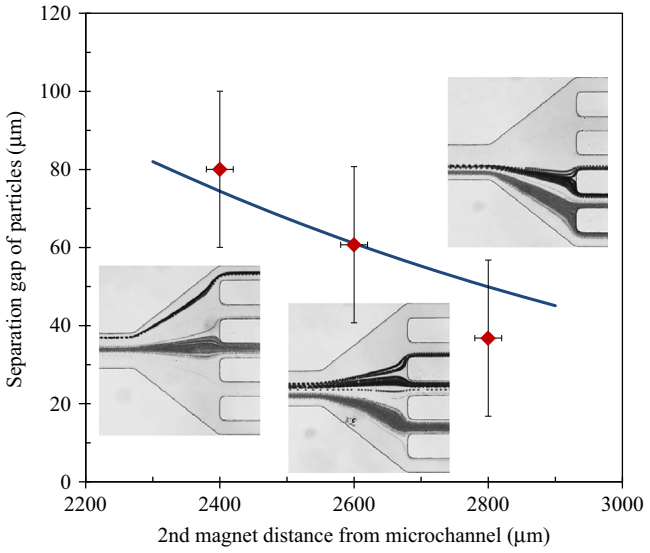

Fig. 5. Effects of the second magnet-microchannel distance on the magnetic separation of 3 μm and 10 μm polystyrene particles in 0.05 × EMG 408 ferrofluid at a fixed speed of 1.2 mm/s. The first magnet-microchannel distance is fixed at 500 μm. The symbols represent the center-to-center distances of the sorted particle streams measured directly from the corresponding streak images at the microchannel outlet (see the insets). The solid line presents the theoretically predicted separation gap from the analytical model.

outlet (right) of the microchannel. The experimental conditions including device and ferrofluid parameters are exactly the same as those for polystyrene particle separation in Fig. 3 except that 3 μm particles in the latter are replaced with yeast cells. As compared with the particle separation image in Fig. 3(c), one can see that the deflection of 10 μm particles at the channel outlet remains similar

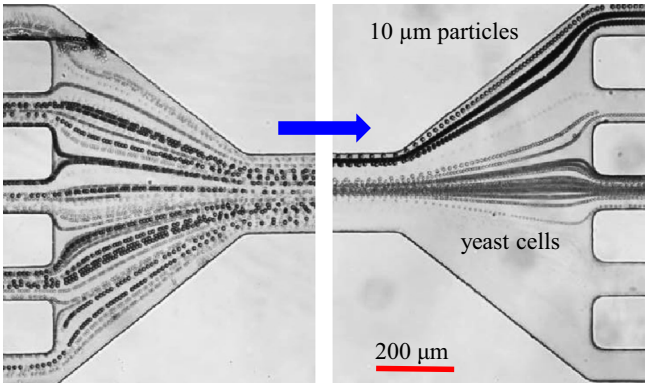

Fig. 6. Streak images at the microchannel inlet (left) and outlet (right) illustrating the continuous magnetic separation of live yeast cells and 10 μm polystyrene particles in 0.05 × EMG 408 ferrofluid with an average flow speed of 0.6 mm/s. The first and second magnets are placed 500 μm and 2600 μm away from the channel edge, respectively. The block arrow indicates the flow direction.

to that in the particle/cell separation image in Fig. 6 (right panel). The magnetic deflection of yeast cells, which appear as gray hollow spheres with a measured average diameter of 5 μm due to their transparent membrane, is, as expected, noticeably greater than that of 3 μm particles in Fig. 3(c). We also simulated the magnetic transport and separation of this yeast cell/particle mixture under the experimental conditions using the analytical model. The predicted cell and particle trajectories (data not shown) are again consistent with the experimental images. The yeast cells collected after the separation experiment were tested for viability using a method described in our earlier papers [44,52]. The results show an overall positive biocompatibility for cell separation in a diluted ferrofluid.

5. Conclusions

We have developed a simple magnetic technique to separate diamagnetic particles and cells in ferrofluid flow through a straight microchannel. Two permanent magnets, which are offset to each other along the channel length with dissimilar magnet-channel distances, are used to achieve a sheath-free focusing and a continuous-flow separation of particles, through the induced negative magnetophoretic deflection. This technique has been demonstrated by separating 3 μm- and 10 μm-diameter polystyrene particles in a diluted ferrofluid. The effects of flow speed and magnet position on the particle separation are examined. The technique has also been applied to separate live yeast cells from 10 μm polystyrene particles followed by a positive biocompatibility test. Moreover, we have developed a 3D analytical model to simulate the magnetic control of particle transport and separation in ferrofluid microflows under the experiment conditions. The predictions are found to agree with the experimental results quantitatively. This demonstrated diamagnetic particle and cell separation technique is noted to have the flexibility of varying the position of the second magnet during experiment for accommodating particles and cells of various sizes.

Acknowledgment

This work was supported by NSF under grant CBET-1150670 (Xuan) and by Clemson University through the University Research Grant (Xuan and Tzeng).

References

[1] R. Pethig, Review article—dielectrophoresis: status of the theory, technology, and applications, Biomicrofluidics 4 (2010) 022811.
[2] J. Regtmeier, R. Eichhorn, M. Viefhues, L. Ogunovic, D. Anselmetti, Electrodeless dielectrophoresis for bioanalysis: theory, devices and applications, Electrophoresis 32 (2011) 2253–2273.
[3] M.A.M. Gijs, Magnetic bead handling on-chip: new opportunities for analytical applications, Microfluidics and Nanofluidics 1 (2004) 22–40.
[4] N. Pamme, Magnetism and microfluidics, Lab on a Chip 6 (2006) 24–38.
[5] T. Laurell, F. Petersson, A. Nilsson, Chip integrated strategies for acoustic separation and manipulation of cells and particles, Chemical Society Reviews 36 (2007) 492–506.
[6] S.C. Lin, X. Mao, T.J. Huang, Surface acoustic wave (SAW) acoustophoresis: now and beyond, Lab on a Chip 12 (2012) 2766–2770.
[7] S.H. Cho, J.M. Godin, C. Chen, W. Qiao, H. Lee, Y. Lo, Review article: recent advancements in optofluidic flow cytometer, Biomicrofluidics 4 (2010) 043001.
[8] A.A. Kayani, K. Khoshmanesh, S.A. Ward, A. Mitchell, K. Kalantar-zadeh, Optofluidics incorporating actively controlled micro- and nano-particles, Biomicrofluidics 4 (2012) 031501.
[9] H. Tsutsui, C.M. Ho, Cell separation by non-inertial force fields in microfluidic systems, Mechanics Research Communications 36 (2009) 92–103.
[10] D. Di Carlo, Inertial microfluidics, Lab on a Chip 9 (2009) 3038–3046.
[11] N. Pamme, Continuous flow separations in microfluidic devices, Lab on a Chip 7 (2007) 1644–1659.
[12] A. Lenshof, T. Laurell, Continuous separation of cells and particles in microfluidic systems, Chemical Society Reviews 39 (2010) 1203–1217.
[13] A.A.S. Bhagat, H. Bow, H. Hou, S. Tan, J. Han, C. Lim, Microfluidics for cell separation, Medical & Biological Engineering & Computing 48 (2010) 999–1014.
[14] D.R. Gossett, W.M. Weaver, A.J. Mach, S.C. Hur, H.T. Tse, W. Lee, H. Amini, D. Di Carlo, Label-free cell separation and sorting in microfluidic systems, Analytical and Bioanalytical Chemistry 297 (2010) 3249–3267.
[15] A. Karimi, S. Yazai, A.M. Ardekani, Hydrodynamic mechanisms of cell and particle trapping in microfluidics, Biomicrofluidics 7 (2013) 021501.
[16] C. Liu, T. Stakenborg, S. Peeters, L. Lagae, Cell manipulation with magnetic particles toward microfluidic cytometry, Journal of Applied Physics 105 (2009) 102011–102014.
[17] M. Suwa, H. Watarai, Magnetoanalysis of micro/nanoparticles: a review, Analytica Chimica Acta 690 (2011) 137–147.
[18] N.T. Nguyen, Micro-magnetofluidics: interactions between magnetism and fluid flow on the microscale, Microfluidics and Nanofluidics 12 (2012) 1–16.
[19] Q. Ramadan, M.A.M. Gijs, Microfluidic applications of functionalized magnetic particles for environmental analysis: focus on waterborne pathogen detection, Microfluidics and Nanofluidics 13 (2012) 529–542.
[20] R.M. Erb, B. Yellen, Magnetic manipulation of colloidal particles, in: J.P. Liu (Ed.), Nanoscale Magnetic Materials and Applications, Springer, New York, 2009.
[21] M.A.M. Gijs, F. Lacharme, U. Lehmann, Microfluidic applications of magnetic particles for biological analysis and catalysis, Chemical Reviews 110 (2010) 1518–1563.
[22] M. Zborowski, J.J. Chalmers, Rare cell separation and analysis by magnetic sorting, Analytical Chemistry 83 (2011) 8050–8056.
[23] K. Hoshino, Y.Y. Huang, N. Lane, M. Huebschman, J.W. Uhr, E.P. Frenkel, X. Zhang, Microchip-based immunomagnetic detection of circulating tumor cells, Lab on a Chip 11 (2011) 3449–3457.
[24] J.H. Kang, S. Krause, H. Tobin, A. Mammoto, M. Kanapathipillai, D.E. Ingber, A combined micromagnetic–microfluidic device for rapid capture and culture of rare circulating tumor cells, Lab on a Chip 12 (2012) 2175–2181.
[25] B. Schmitz, A. Radbruch, T. Kümmel, C. Wickenhauser, H. Korb, M. L. Hansmann, J. Thiele, R. Fischer, Magnetic activated cell sorting (MACS)—a new immunomagnetic method for megakaryocytic cell isolation: comparison of different separation techniques, European Journal of Haematology 52 (1994) 267–275.
[26] B.B. Yellen, R.M. Erb, H.S. Son, R. Hewlin Jr., H. Shang, G.U. Lee, Traveling wave magnetophoresis for high resolution chip based separations, Lab on a Chip 7 (2007) 1681–1688.
[27] A.R. Kose, B. Fischer, L. Mao, H. Koser, Label-free cellular manipulation and sorting via biocompatible ferrofluids, Proceedings of the National Academy of Sciences USA 106 (2009) 21478–21483.
[28] M. Zborowski, L. Sun, L.R. Moore, P.S. Williams, J.J. Chalmers, Continuous cell separation using novel magnetic quadrupole flow sorter, Journal of Magnetism and Magnetic Materials 194 (1999) 224–230.
[29] C.W. Yung, J. Fiering, A.J. Mueller, D.E. Ingber, Micromagnetic–microfluidic blood cleansing device, Lab on a Chip 9 (2009) 1171–1177.
[30] M. Hoyos, L. Moore, P.S. Williams, M. Zborowski, The use of a linear Halbach array combined with a step-SPLITT channel for continuous sorting of magnetic species, Journal of Magnetism and Magnetic Materials 323 (2011) 1384–1388.
[31] N. Xia, T.P. Hunt, B.T. Mayers, E. Alsberg, G.M. Whitesides, R.M. Westervelt, D. E. Ingber, Combined microfluidic–micromagnetic separation of living, Biomedical Microdevices 8 (2006) 299–308.
[32] S. Shen, H. Hwang, Y.K. Hahn, J.K. Park, Label-free cell separation using a tunable magnetophoretic repulsion force, Analytical Chemistry 84 (2012) 3075–3081.

[33] S. Kim, S.I. Han, M.J. Park, C.W. Jeon, Y.D. Joo, I.H. Choi, K.H. Han, Circulating tumor cell microseparator based on lateral magnetophoresis and immunomagnetic nanobeads, Analytical Chemistry 86 (2013) 2779–2786.
[34] N. Pamme, J.C.T. Eijkel, A. Manz, On-chip free-flow magnetophoresis: separation and detection of mixtures of magnetic particles in continuous flow, Journal of Magnetism and Magnetic Materials 307 (2006) 237–244.
[35] N. Pamme, C. Wilhelm, Continuous sorting of magnetic cells via on-chip free-flow magnetophoresis, Lab on a Chip 6 (2006) 974–980.
[36] M.D. Tarn, S.A. Peyman, D. Robert, A. Iles, C. Wilhelm, N. Pamme, The importance of particle type selection and temperature control for on-chip free-flow magnetophoresis, Journal of Magnetism and Magnetic Materials 321 (2009) 4115–4122.
[37] D. Roberta, N. Pamme, H. Conjeauda, F. Gazeaua, A. Ilesb, C. Wilhelm, Cell sorting by endocytotic capacity in a microfluidic magnetophoresis device, Lab on a Chip 11 (2011) 1902–1910.
[38] J.D. Adams, U. Kim, H.T. Soh, Multi-target magnetic activated cell sorter (MT-MACS), Proceedings of the National Academy of Sciences USA 105 (2008) 18165–18170.
[39] S.A. Peyman, E.Y. Kwan, O. Margarson, A. Iles, N. Pamme, Diamagnetic repulsion—a versatile tool for label-free particle handling in microfluidic devices, Journal of Chromatography A 1216 (2009) 9055–9062.
[40] M. Vojtisek, M.D. Tarn, N. Hirota, N. Pamme, Microfluidic devices in superconducting magnets: on-chip free-flow diamagnetophoresis of polymer particles and bubbles, Microfluidics and Nanofluidics 13 (2012) 625–635.
[41] T. Zhu, F. Marrero, L. Mao, Continuous separation of non-magnetic particles inside ferrofluids, Microfluidics and Nanofluidics 9 (2010) 1003–1009.
[42] T. Zhu, R. Cheng, S.A. Lee, E. Rajaraman, M.A. Eiteman, T.D. Querec, E.R. Unger, L. Mao, Continuous-flow ferrohydrodynamic sorting of particles and cells in microfluidic devices, Microfluidics and Nanofluidics 13 (2012) 645–654.
[43] L. Liang, X. Xuan, Continuous sheath-free magnetic separation of particles in a U-shaped microchannel, Biomicrofluidics 6 (2012) 044106.
[44] J. Zeng, C. Chen, P. Vedantam, V. Brown, T. Tzeng, X. Xuan, Three-dimensional magnetic focusing of particles and cells in ferrofluid flow through a straight microchannel, Journal of Micromechanics and Microengineering 22 (2012) 105018.
[45] L. Liang, J. Zhu, X. Xuan, Three-dimensional diamagnetic particle deflection in ferrofluid microchannel flows, Biomicrofluidics 5 (2011) 034110.
[46] L. Liang, X. Xuan, Diamagnetic particle focusing in ferromicrofluidics using a single magnet, Microfluidics and Nanofluidics 13 (2012) 637–643.
[47] T. Zhu, D.J. Lichlyter, M.A. Haidekker, L. Mao, Analytical model of microfluidic transport of non-magnetic particles in ferrofluids under the influence of a permanent magnet, Microfluidics and Nanofluidics 10 (2011) 1233–1245.
[48] T. Zhu, R. Cheng, L. Mao, Focusing microparticles in a microchannel with ferrofluids, Microfluidics and Nanofluidics 11 (2011) 695–701.
[49] J. Zhu, L. Liang, X. Xuan, On-chip manipulation of nonmagnetic particles in paramagnetic solution using embedded permanent magnets, Microfluidics and Nanofluidics 12 (2012) 65–73.
[50] R.E. Rosensweig, Magnetic fluids, Annual Review of Fluid Mechanics 19 (1987) 437–463.
[51] E.P. Furlani, Permanent Magnet and Electromechanical Devices: Materials, Analysis, and Applications, Academic Press, London, 2001.
[52] J. Zeng, C. Chen, P. Vedantam, T.R. Tzeng, X. Xuan, Magnetic concentration of particles and cells in ferrofluid flow through a straight microchannel using attracting magnets, Microfluidics and Nanofluidics (2013), http://dx.doi.org/10.1007/s10404-012-1126-0. (in press).